Molecular pathway underlying bouton stabilization by Semaphorin4D during inhibitory synapse formation

Cátia P. Frias[1], Tom Bresser[1], Lisa Scheefhals[1], Paul M. P. van Bergen en Henegouwen[1], Casper C. Hoogenraad[1] and Corette J. Wierenga[1*]

[1]Cell Biology, Department of Biology, Faculty of Science, Utrecht University, Utrecht, the Netherlands

*Corresponding author:
Corette J. Wierenga
Cell Biology, Department of Biology, Faculty of Science, Utrecht University, Padualaan 8, 3584CH Utrecht, The Netherlands
E-mail: c.j.wierenga@uu.nl
Tel. +31-30-253 2659

Number of figures:	5
Number of supplementary figures:	4
Number of words in the abstract:	147
Number of pages:	36

ABSTRACT

Changes in inhibitory connections are essential for experience-dependent circuit adaptations, and inhibitory defects may underlie neurodevelopmental diseases such as autism. Inhibitory axons and their presynaptic boutons can undergo rapid changes, but the molecular mechanisms underlying these dynamics and their role in inhibitory synapse formation are currently unclear. By monitoring inhibitory axons over time in organotypic hippocampal slices, we show that stabilization of presynaptic boutons is the first step in inhibitory synapse formation and that this process is regulated by the guidance protein Semaphorin4D (Sema4D). Sema4D signaling induces inhibitory bouton stabilization within tens of minutes without affecting bouton disassembly. We show that this signaling pathway requires ongoing neuronal activity, and involves activation of receptor tyrosine kinase MET and actin remodeling. Our data indicate that actin plays an important role during synapse formation and demonstrate a novel link between MET, a known autism risk factor, and inhibitory presynaptic dynamics.

INTRODUCTION

For proper information processing during the ongoing stream of events in life, synaptic connections in the brain are continuously updated. Recent imaging studies have demonstrated that axons and their presynaptic terminals (e.g. boutons) are highly dynamic structures that can rapidly adapt to changes. Intra-axonal exchange of synaptic vesicles occurs between neighboring boutons at a time scale of minutes (Staras, 2007) and entire boutons can appear, disappear and reappear over the course of minutes to hours (Sabo et al., 2006, Wierenga et al., 2008). These ongoing axonal dynamics are thought to allow quick implementation of synaptic changes in response to activity changes or other environmental signals (Staras, 2007, Frias and Wierenga, 2013). Inhibitory axons appear particularly dynamic (Fu et al., 2012, Schuemann et al., 2013, Keck et al., 2011, Chen et al., 2015). Rapid inhibitory adaptation can serve as a gating mechanism for plasticity at nearby excitatory synapses, which occurs at a slower time scale (Chen et al., 2015, Froemke et al., 2007, Keck et al., 2011, Villa et al., 2016), and this may be an important aspect of circuit development and adaptation (Hensch, 2005, Froemke, 2015). We currently do not understand the molecular processes taking place during rapid adaptation of inhibitory axons and how these are regulated.

We previously showed that new inhibitory synapses form by the occurrence of new presynaptic boutons at pre-existing axon-dendrite crossings (Wierenga et al., 2008, Schuemann et al., 2013). The apparently stochastic dynamics of inhibitory boutons during this process seem to contrast with studies in which a local signaling event, such as specific adhesion between the pre- and postsynaptic membranes, is followed by recruitment of presynaptic proteins and synaptic vesicles within minutes (Siddiqui and Craig, 2011, Wierenga, 2016). In studies using heterologous culture systems, presynaptic assembly may occur as a sequential process, but it is important to understand the sequence of events that takes place during synapse formation in intact tissue.

The class 4 semaphorin Sema4D has recently been shown to signal rapid changes in inhibitory synapses. Knockdown of postsynaptic Sema4D leads to a reduction in the density of GABAergic synapses (Paradis et al., 2007), while addition of soluble Sema4D to primary hippocampal cultures induces rapid formation of functional inhibitory synapses (Kuzirian et al., 2013). It was shown that Sema4D acts as a postsynaptic protein and requires only its

extracellular domain to induce inhibitory synapses through its receptor PlexinB1 (Kuzirian et al., 2013, Raissi et al., 2013). However, the Sema4D/PlexinB1 signaling pathway in inhibitory axons is not understood. In neuronal and non-neuronal cells, Sema4D signaling through PlexinB1 induces signal cascades involving small GTPases (Vodrazka et al., 2009, Oinuma et al., 2004). Depending on the association of PlexinB1 with receptor tyrosine kinases, different downstream signal cascades can be activated , which can have opposing effects on the actin cytoskeleton (Tasaka et al., 2012, Swiercz et al., 2002). It is currently not clear how actin remodeling is linked with signaling molecules at the membrane and synapse formation.

In the current study, we examine the link between Sema4D signaling and actin in regulating the dynamics of inhibitory synapse formation. We find that Sema4D signaling regulates stabilization of inhibitory boutons along the axon, one of the early steps in inhibitory synapse formation. We further characterized the molecular pathway of Sema4D-induced bouton stabilization and found that it is activity-dependent, involves actin remodeling, and requires the activation of the receptor tyrosine kinase MET. Our results elucidate an important regulatory pathway of activity-dependent inhibitory synapse formation and identify bouton stabilization by actin remodeling as one of the earliest events in this process.

RESULTS

We performed time-lapse two-photon microscopy in organotypic hippocampal cultures from GAD65-GFP mice to monitor the dynamics of inhibitory boutons in the CA1 region of the hippocampus (Schuemann et al., 2013, Wierenga et al., 2008). High-resolution image stacks of GFP-labelled inhibitory axons were acquired every 10 minutes, for a total period of 150 minutes. We have previously shown that inhibitory boutons are highly dynamic and appear, disappear and reappear during the course of hours (Schuemann et al., 2013, Wierenga et al., 2008). To bias our analysis towards synaptic events, we only included boutons that appeared for at least 2 time points at the same location during the imaging period in our analysis (Schuemann et al., 2013). We distinguished two main classes of boutons: persistent boutons were present during all time points, while non-persistent boutons were absent during one or more time points during the imaging session (Fig. 1A,B). Persistent boutons reflect inhibitory synapses (Fig. 1E) (Müllner et al., 2015, Wierenga et al., 2008) and comprised approximately 60% of total imaged boutons that appeared during the total imaging period (Fig. 1C). This corresponds to approximately 77 % (with standard deviation of 12 %) of boutons at any given time point being persistent. Non-persistent boutons reflect locations where inhibitory synapses are formed or disassembled (Schuemann et al., 2013, Wierenga et al., 2008). Based on the presence or absence of non-persistent boutons during a baseline and wash-in period (details are given in the methods section), we distinguished 5 subgroups of non-persistent boutons: new (N; absent during baseline), lost (L; absent during wash-in), stabilizing (S; non-persistent during baseline, persistent during wash-in), destabilizing (D; persistent during baseline, non-persistent during wash-in) and transient (non-persistent in both periods). These different subgroups of non-persistent boutons not only differed in their incidence and the duration of their presence (Fig. 1C,D), but also in their presynaptic vesicular GABA transporter (VGAT) content (Fig. 1E). Association with VGAT of stabilizing boutons, which were present for at least 90 minutes before fixation, was not different from persistent boutons, indicating that nascent inhibitory synapses are able to recruit synaptic vesicles within this period. On the other hand, new boutons, which were present for a shorter period before fixation, showed a lower percentage of VGAT association. These data show that inhibitory presynaptic boutons are dynamic structures that are continuously being formed

and disassembled along the axons, and suggest that non-persistent boutons reflect boutons at different stages of inhibitory synapse assembly and disassembly.

Inhibitory bouton stabilization during treatment with Sema4D

It was recently shown that class 4 semaphorin Sema4D can rapidly induce the assembly of functional inhibitory synapses in hippocampal dissociated cultures (Kuzirian et al., 2013), but the underlying mechanisms remain unknown. To examine the effect of Sema4D on inhibitory bouton dynamics, we bath applied the extracellular domain of mouse Sema4D conjugated to the Fc region of mouse IgG2A (Sema4D; 1 nM) and compared inhibitory bouton dynamics during a baseline period of 5 time points and during Sema4D treatment in the subsequent 10 time points (Fig. 2A). We used Fc alone (1 nM) as a control (Kuzirian et al., 2013). Bath application of Sema4D did not affect overall axonal morphology (Fig. 2A), and did not change the density of inhibitory boutons (Fig. 2B). However, when we analyzed the different subgroups of non-persistent boutons, we found that Sema4D treatment specifically enhanced the fraction of stabilizing boutons, while leaving all other subgroups unaffected (Fig. 2C, Fig. S1A-E). Indeed, treatment with Sema4D induced a >2-fold increase in the absolute density of stabilizing boutons (Fig. 2D). To examine how Sema4D-induced stabilization developed over time, we quantified the number of non-persistent boutons that were present for 5 consecutive time points during the baseline and the wash-in period. We found that Sema4D induced a marked increase in bouton stabilization over the course of the wash-in period (Fig. 2E), and strongly enhanced the number of boutons that had stabilized at the end of this period (last 5 time points; Fig. 2F). Stabilizing boutons are relatively rare in our slices and under control conditions only 40% of the axons display one or more stabilizing boutons. Treatment with Sema4D significantly increased this fraction to 77% (Fig. 2G). Altogether, these data show that Sema4D treatment rapidly and specifically promotes the stabilization of inhibitory boutons, without affecting bouton disassembly.

Sema4D-induced bouton stabilization relies on network activity

We previously showed that inhibitory bouton dynamics are affected by neuronal activity (Schuemann et al., 2013), suggesting that the process of bouton stabilization may be affected by ongoing network activity under control conditions. We therefore determined whether the Sema4D-induced stabilization of inhibitory boutons depended on network

activity. As expected (Schuemann et al., 2013), blocking activity with tetrodotoxin (TTX) only slightly decreased overall bouton dynamics in our slices (Fig. S1F). However, we found that in the presence of TTX Sema4D did no longer induce stabilization of inhibitory boutons, even leading to a reduction in bouton stabilization compared to control (Fig. 2H,I) and decreased the density of lost boutons (Fig. S1G). These findings show that Sema4D treatment had a differential effect on bouton dynamics depending on neuronal activity levels and indicate that Sema4D requires active neuronal networks to promote the stabilization of inhibitory presynaptic boutons.

Sema4D-induced stabilization of inhibitory boutons precedes inhibitory synapse formation

We next assessed whether Sema4D-induced bouton stabilization leads to the formation of new inhibitory synapses. We first examined if longer Sema4D treatment enhances the bouton stabilization effect. We compared dynamics of individual boutons during baseline and after 6h treatment (400 minutes total treatment) and found that longer Sema4D treatment also induced prominent bouton stabilization (Fig. 3A). However, the 6 h treatment did not increase bouton stabilization beyond the 2 h treatment (Fig. 3B), suggesting that the number of inhibitory boutons that can be stabilized by Sema4D is limited. In addition to promoting bouton stabilization, longer treatments also induced a reduction in the density of transient boutons (Fig. 3C). This secondary effect was only revealed by analyzing the effect over time, suggesting a more general reduction of dynamics as an indirect effect of prolonged bouton stabilization. These results indicate that the Sema4D-induced stabilization of inhibitory boutons persists, but does not further increase, with longer treatments.

We next asked if Sema4D-induced inhibitory bouton stabilization leads to the formation of new synapses. We treated organotypic hippocampal slices with 1 nM Fc or 1nM Sema4D for 2, 6 and 24 h, and determined overall inhibitory synapse density by immunohistochemistry. We used antibodies against presynaptic VGAT and postsynaptic gephyrin to visualize inhibitory synapses (Fig. 3D,E). Indeed, Sema4D induced a clear increase in the density of inhibitory synapses after 24 h (Fig. 3F). Treatment with Sema4D induced an increase in the area of VGAT puncta, without affecting their density (Fig. 3G,H). For gephyrin, Sema4D treatment caused an increase in puncta density, but not in their size (Fig. 3I,J). The average puncta intensity was not affected (at 24h, VGAT: 107 % ± 4 % of control, p= 0.34 (MW); gephyrin: 106 % ± 5 % of control, p = 0.5 (MW)). Interestingly, the time course for

presynaptic and postsynaptic changes was different. Whereas the increase in presynaptic VGAT area could be detected after 6 h, the increase in postsynaptic gephyrin density was only evident after 24 h. Note that the increase in presynaptic VGAT could already be detected in individual boutons after 2 h (Fig. 1E). The slower postsynaptic response compared to a previous report in primary cultures (Kuzirian et al., 2013) may reflect a difference in overall neuronal maturation (Oh et al., 2016). Together, these data indicate that the initial Sema4D-induced stabilization of inhibitory boutons is followed by a slower maturation process, through an increase in presynaptic vesicle content and subsequent acquisition of postsynaptic scaffolds (Dobie and Craig, 2011, Wierenga et al., 2008).

Actin remodeling by low doses of LatrunculinB promotes stabilization of inhibitory boutons

The assembly of inhibitory synapses induced by Sema4D in dissociated hippocampal neurons was shown to be dependent on its receptor PlexinB1 (Kuzirian et al., 2013), and PlexinB1 activation can induce changes in actin (Tasaka et al., 2012, Swiercz et al., 2002). To examine how the actin cytoskeleton is involved in inhibitory bouton dynamics, we studied the effect of the actin monomer sequestering drug LatrunculinB (LatB) and the actin filament stabilizer drug Jasplakinolide (Jasp) in our system. In the low concentrations that we use here (100 nM LatB and 200 nM Jasp) these drugs perturb the actin cytoskeleton without affecting synaptic function (Rex et al., 2009, Honkura et al., 2008). None of the treatments changed overall axon morphology (Fig. 4A). We found that both actin regulators appeared to promote overall dynamics of inhibitory boutons, as was suggested from a trend towards an increase in new and transient boutons (Fig. 4B-E and S2). However, these drugs showed clear distinctive effects on stabilizing boutons. While Jasp did not appear to affect stabilizing boutons (Fig. 4C), we found that LatB treatment resulted in a specific increase in the absolute density of stabilizing boutons by almost 2-fold (Fig. 4F,G). These findings show that inhibitory bouton dynamics are regulated by changes in the actin cytoskeleton. Moreover, we found that treatment with LatB mimics Sema4D-induced stabilization of inhibitory boutons, suggesting a common underlying pathway.

MET is enriched at a subset of inhibitory presynaptic boutons

The outcome of Sema4D/PlexinB1 signaling on the underlying actin cytoskeleton relies on the co-activation of receptor tyrosine kinase receptors. Co-activation of MET upon Sema4D treatment has been shown to promote anti-migratory effects in some breast cancer lines through actin remodeling by the inactivation of small RhoGTPase RhoA (Swiercz et al., 2008, Sun et al., 2012). Based on the observed similarity between Sema4D and LatB treatment on inhibitory bouton dynamics, we wondered if MET plays a role in Sema4D-induced bouton stabilization. MET has previously been shown to be enriched in axonal tracts and to co-localize with presynaptic markers of excitatory synapses (Eagleson et al., 2013, Judson et al., 2009), but its presence at inhibitory synapses is debated. To address a possible localization of MET at inhibitory synapses, we made use of a nanobody against MET (Heukers et al., 2014). We confirmed that this nanobody labels synapses in primary hippocampal cultures (Fig. S3A). The majority of MET puncta overlapped with excitatory synapses as previously reported (Eagleson et al., 2013, Tyndall and Walikonis, 2006), but clear association of MET with inhibitory presynapses was also observed (Fig. S3B). When we labeled MET in our hippocampal slices of GAD65-GFP mice, we observed that 21 % ± 3 % of the GFP-labeled inhibitory boutons were enriched for MET (Fig. 5A-C). Comparing the MET staining pattern with staining for postsynaptic gephyrin (compare Fig. 5B with Fig. 3E) suggests a presynaptic localization of MET at these inhibitory synapses. Together, these data show that with our method we are able to detect enrichment of MET in a subset of inhibitory presynaptic boutons.

Inhibitory bouton stabilization by Sema4D requires MET

We next assessed if MET activation is necessary for the observed Sema4D-induced stabilization of boutons. After the baseline period, we treated our slices with Sema4D as before or in combination with PHA-665752 (PHA), a highly specific MET inhibitor (Lim and Walikonis, 2008). We observed that adding the PHA blocker alone did not affect bouton dynamics (Fig. S3C-D), suggesting that MET is not activated under baseline conditions in our slices. However, blocking MET completely abolished the Sema4D-induced increase in the density of stabilizing boutons (Fig. 5D). In fact, blocking MET almost entirely abolished the occurrence of stabilizing boutons (Fig. 5E). Sema4D treatment in the presence of PHA had only a mild effect on the other bouton subgroups (Fig. S4). Consistent with the live imaging data, inhibiting MET with PHA also blocked the increase in VGAT staining intensity after

248 Sema4D treatment (Fig. 5F,G). Taken together, these data indicate that activation of MET is
249 required for the Sema4D-induced stabilization of inhibitory boutons.

250

DISCUSSION

Our live imaging experiments give unique insight in the dynamics of the process of inhibitory synapse formation in brain slices, which would have remained undetected with methods using stationary comparisons before and after treatment. Our data demonstrate that presynaptic bouton stabilization is an important early step during inhibitory synapse formation and we characterized the molecular pathway by which the guidance protein Sema4D regulates this process. We show that actin remodeling plays an important role in inhibitory bouton dynamics and reveal a novel role for the receptor tyrosine kinase MET in inhibitory synapses.

In postnatal brain tissue, in which the majority of inhibitory connections have been established, synapse formation and disassembly is still ongoing. In our slices, many GFP-labelled boutons are persistent and display pre- and postsynaptic markers of mature inhibitory synapses, but a significant portion of inhibitory boutons are non-persistent and they reflect a subset of non-mature synapses. Non-persistent boutons represent locations where inhibitory synapses can be formed, but where the outcome (e.g. synapse formation or not) is still undecided (Fu et al., 2012, Kuriu et al., 2012, Schuemann et al., 2013, Wierenga et al., 2008). We found that Sema4D-induced stabilization only affected a subset of non-persistent inhibitory boutons and that longer treatment (>2 hr) did not further increase bouton stabilization, suggesting the involvement of Sema4D signaling only at a specific stage of synapse formation. Our data demonstrate that Sema4D signaling specifically promotes the stabilization of inhibitory boutons at pre-defined locations, but that it cannot induce formation of synapses *de novo*. Destabilization and disassembly of inhibitory synapses were also not affected by Sema4D, indicating that formation and disassembly of inhibitory synapses are independently regulated processes. Our data suggest that signaling pathways can interfere at different steps of inhibitory synapse formation in a highly specific manner.

Our results show that the dynamics of inhibitory boutons is regulated by intracellular modification of actin structures. It has been previously shown that bouton dynamics reflect intra-axonal transport of presynaptic components, including clusters of synaptic vesicles and

active zone components (Staras, 2007, Sabo et al., 2006, Fu et al., 2012). Our observation that Sema4D and LatB induce similar bouton stabilization suggests that both treatments induce similar changes in immature boutons and that the affinity for vesicle capture may be defined by local actin structures. Low doses of monomer sequestering drugs, such as LatB used in our study, presumably do not lead to the complete disassembly of actin structures (Bleckert et al., 2012, Honkura et al., 2008, Ganguly et al., 2015). Instead, limited availability of actin monomers may indirectly affect actin-regulating factors resulting in structural changes of the actin cytoskeleton (Ganguly et al., 2015, Suarez et al., 2015). Future studies will be needed to unravel precise actin structures and the role of actin-regulating factors in axonal boutons, and the specific changes that occur during synapse formation.

Although the importance of the actin cytoskeleton in regulating synaptic function has been clearly shown (Cingolani and Goda, 2008, Nelson et al., 2013), it has been less clear if actin is involved during synapse formation. Our data indicate that presynaptic actin remodeling is one of the first events occurring during inhibitory synapse formation. This finding is supported by two recent studies that show a similar role for actin in synaptogenesis in *C. elegans* (Chia et al., 2014) and *Drosophila* (Piccioli and Littleton, 2014). In these studies, local axonal actin remodeling is followed by the subsequent recruitment of pre- and postsynaptic organizing molecules at nascent synapses. It is currently not known if additional signals are needed to transform stabilized boutons into mature inhibitory synapses in mammalian tissue.

Sema4D is a member of the family of semaphorin guidance molecules and plays several roles in development of the brain and the immune system (Swiercz et al., 2002, Shi et al., 2000). Sema4D signaling can activate multiple intracellular pathways through its receptor plexinB1 (Oinuma et al., 2004, Vodrazka et al., 2009). In this study, we found that activation of the receptor tyrosine kinase MET is required for Sema4D-induced inhibitory bouton stabilization. In analogy to what has been described in non-neuronal cells, we propose that MET acts as a co-receptor for the Sema4D receptor PlexinB1 (Kuzirian et al., 2013, Swiercz et al., 2008), promoting an intracellular pathway downstream of Sema4D binding that ultimately leads to actin remodeling within the axon. Consistent with this scenario, we found that MET is enriched in a subset of inhibitory synapses, both in primary hippocampal cultures and organotypic slices. Previous studies have implicated MET in regulating postsynaptic strength

in excitatory neurons (Lo et al., 2016, Qiu et al., 2014), and in interneuron migration during early stages of neuronal development (Martins et al., 2011). Our data indicate a novel role for MET in the assembly of inhibitory presynapses.

Our observation that Sema4D-induced bouton stabilization required ongoing neuronal activity suggests that this process plays a role during activity-dependent inhibitory plasticity. A number of recent papers have described a rapid response of inhibitory axons to changes in activity levels (Schuemann et al., 2013) and $GABA_B$ signaling (Fu et al., 2012) *in vitro*, as well as to sensory deprivation (Keck et al., 2011) and motor learning (Chen et al., 2015) *in vivo*. The fast inhibitory response may serve as a gating mechanism for plasticity at nearby excitatory synapses, which takes place at a slower time scale (Froemke, 2015, Froemke et al., 2007, Hensch, 2005, Keck et al., 2011, Villa et al., 2016). These reports suggest that rapid modulation of levels of inhibition may be a general feature of experience-dependent adjustment of neuronal networks during development and learning. Defects in inhibitory adaptation may contribute to neurodevelopmental disorders, including autism spectrum disorder (ASD). It is therefore interesting that the MET gene is an established risk factor for ASD, as determined by various human imaging and genetic studies (Peng et al., 2013). Together, our results elucidate an important regulatory pathway of inhibitory synapse formation that is relevant for experience-dependent circuit adaptation, and it will be important to examine how these pathways are affected in ASD mouse models in the future.

METHODS

Animals

All animal experiments were performed in compliance with the guidelines for the welfare of experimental animals issued by the Federal Government of The Netherlands. All animal experiments were approved by the Animal Ethical Review Committee (DEC) of Utrecht University.

Hippocampal slice cultures

Hippocampal slice cultures (400 µm thick) were prepared from postnatal day 5-7 of both male and female GAD65-GFP mice (Lopez-Bendito et al., 2004) as previously described (Müllner et al., 2015). In short, the hippocampi were dissected in ice-cold HEPES-GBSS (containing 1.5 mM $CaCl_2 \cdot 2H_2O$, 0.2 mM KH_2PO_4, 0.3 mM $MgSO_4 \cdot 7H_2O$, 5 mM KCl, 1 mM $MgCl_2 \cdot 6H_2O$, 137 mM NaCl, 0.85 mM Na_2HPO_4 and 12.5 mM HEPES) supplemented with 1 mM kynurenic acid and 25 mM glucose, and plated in a MEM-based medium (MEM supplemented with 25 % HBSS, 25 % horse serum, 30 mM glucose and 12.5 mM HEPES).

In GAD65-GFP mice, approximately 20% of the CA1 interneurons express GFP from early embryonic developmental stage into adulthood (Lopez-Bendito et al., 2004, Wierenga et al., 2010). The majority of GFP-labeled interneurons expresses reelin and VIP, while parvalbumin and somatostatin expression is nearly absent (Wierenga et al., 2010). For our study, the relatively low number of GFP-positive axons is crucial for proper analysis of individual boutons.

The slices were kept in culture for at least one week before the experiments (range 7-18 days *in vitro*) at 35°C in 5 % CO_2. For live imaging experiments, slices were transferred to an imaging chamber, where they were continuously perfused with carbogenated artificial cerebrospinal fluid (ACSF; containing 126 mM NaCl, 3 mM KCl, 2.5 mM $CaCl_2$, 1.3 mM $MgCl_2$, 1.25 mM NaH_2PO_4, 26 mM $NaHCO_3$, 20 mM glucose and 1mM Trolox). The temperature of the chamber was maintained at 37°C. Treatment and control experiments were conducted in slices from sister cultures.

Pharmacological treatments

The following drugs were used: 0.1/0.2 % DMSO, 1 nM Fc and Sema4D-Fc (amino acids 24-711) (both R&D Systems), 100 nM Latrunculin B (Santa Cruz Biotechnology), 200 nM Jasplakinolide (Tocris Bioscience) and 1 µM PHA-665752 (Sigma-Aldrich). We used the small molecule PHA-665752 (PHA), a specific MET inhibitor, to decrease endogenous phosphorylation of MET, without affecting MET expression or neuronal cell viability (Lim and Walikonis, 2008).

For treatments that were followed by immunostaining of inhibitory synapses, 1 nM Fc or Sema4D-Fc was added to the culturing medium and slices were left in the incubator for 2, 6 or 24 h before fixation.

Two-photon imaging

For acute treatments, drugs were added to the perfusion ACSF after a baseline period of 40 minutes (5 time points) and we continued imaging for an additional 10 time points in the treatment period (total imaging period is 140 minutes). In longer treatments, we treated the slices for 6 hours after the baseline period (5 imaging time points) at the microscope and restarted imaging for 5 time points, for a total treatment period of 6 hours and 40 minutes (400 minutes). For activity blockade, 0.5 µM tetrodotoxin citrate (TTX; Tocris Bioscience) was added to the perfusion ACSF prior to the transfer of the slice to the imaging chamber. Time-lapse two-photon microscopy images were acquired on a Femtonics 2D two-photon laser-scanning microscope (Budapest, Hungary), with a Nikon CFI Apochromat 60X NIR water-immersion objective. GFP was excited using a laser beam tuned to 910 nm (Mai Tai HP, Spectra Physics). The 3D images (93.5 µm x 93.5 µm in xy, 1124 x 1124 pixels) consisted of 29-33 z stacks (0.5 µm step size in z). Small misalignments due to drift were manually compensated during the acquisition.

Two-photon image analysis

The analysis of inhibitory bouton dynamics was performed semi-automatically using ImageJ (US National Institute of Health) and Matlab-based software (Mathworks). The 3D coordinates of individual axons were selected at every time point by using the CellCounter plugin (Kurt De Vos, University of Sheffield, Academic Neurology). For each image, 1-5

stretches of axons (average length 78 µm with standard deviation 18 µm) were selected for analysis.

A 3D intensity profile along the selected axons was constructed at each time point, and individual boutons were identified in a two-step process using custom-made Matlab software (Schuemann et al., 2013). In brief, an axon threshold was calculated to differentiate the axon from the background (2 standard deviations above mean intensity); subsequently, a local threshold (0.5 standard deviation above mean axon intensity) identified the boutons along the selected axon. Only boutons with at least 5 pixels above bouton threshold were included. Each image stack was visually examined and false positives and negatives were corrected manually. Only raw data was analyzed; images were median-filtered for illustration purposes only.

Boutons were classified as persistent when they were present during all time points, and non-persistent when they were absent during one or more time points during the imaging session. To bias our analysis towards synaptic events (Schuemann et al., 2013), we restricted our analysis to boutons that appeared for at least 2 time points at the same location during the imaging period. We verified that our main conclusions did not change when this restriction was released. Based on their presence during baseline and wash-in periods, we defined five subgroups of non-persistent boutons: new boutons (not present during baseline), lost boutons (not present during wash-in), stabilizing boutons (non-persistent during baseline, persistent during wash-in), destabilizing boutons (persistent during baseline, non-persistent during wash-in), and transient boutons (non-persistent in baseline and wash-in) (Fig. 1). The duration of each bouton was defined as the number of time points present divided by the total number of time points per period. Bouton density was calculated as the average number of boutons at all time points divided by the 3D axon length. The instantaneous bouton gain (or loss) was defined as the fraction of boutons that were gained (or lost) between two consecutive time points, (Schuemann et al., 2013).

Immunohistochemistry, confocal imaging and image analysis

For *post hoc* immunohistochemistry, organotypic hippocampal slices were fixed in 4 % (w/v) paraformaldehyde for 30 minutes at room temperature. Slices were rinsed in phosphate buffer and permeabilized with 0.5 % TritonX-100 in phosphate buffer for 15 minutes. Slices were then blocked with 0.2 % TritonX-100, 10 % goat serum (ab7481, Abcam) in phosphate

buffer for 60 minutes. Primary antibodies were applied overnight at 4°C in blocking solution. After washing, slices were incubated with secondary antibodies in blocking solution for 4h at room temperature. Slices were then washed and mounted on slides in Vectashield mounting medium (Vector Labs).

The following primary and secondary antibodies were used: rabbit α-VGAT (1:1000; Synaptic Systems, 131 003), mouse α-gephyrin (1:1000; Synaptic Systems, 147 011), guinea pig α-VGLUT (1:400; Millipore, AB5905), rabbit α-Homer (1:1000; Synaptic Systems, 160 002), mouse α-myc (1:100; Oncogene Research Products, OP10), Alexa405-, Alexa-488 and Alexa-568 conjugated secondary antibodies (Invitrogen). For staining MET we used a previously described myc-tagged nanobody, which was shown to recognize MET with low nanomolar affinity (Heukers et al., 2014). We visualized the nanobody with an antibody against the C-terminal myc tag. We validated the nanobody staining in primary hippocampal cultures using a previously described immunostaining protocol (Esteves da Silva et al., 2015).

For immunostainings, high resolution confocal laser scanning microscopy was performed on a Zeiss LSM-700 system with a Plan-Apochromat 63x 1.4 NA oil immersion objective. Each image was a z-series of 11-35 images (0.3 µm z step size), each averaged 4 times. The imaging area in the CA1 region was 78 x 78 µm (1024 x 1024 pixels). The confocal settings were kept the same to compare fluorescence intensities between slices.

For the quantification of VGAT and gephyrin intensities per image, we determined the mean intensity of 3 randomly chosen areas of 10 x 10 µm of the average projection image from the 5 middle z-layers. Synaptic puncta size and number were determined using the PunctaAnalyzer plugin, and inhibitory synapses were defined as overlapping VGAT and gephyrin puncta. For determining co-localization of GFP-labeled boutons with synaptic marker VGAT or with MET, we manually inspected individual boutons through all z-sections. A bouton was only considered positive when at least one z stack of the bouton overlapped with VGAT or MET staining. The images were median-filtered only for illustration purposes.

Statistics

Data are represented as mean values ± standard error of the mean, unless stated otherwise. Statistical analysis was performed using GraphPad Prism software. Results from treatment and control experiments were compared using the Mann-Whitney U test (MW). The Chi-Square test (χ^2) was used for comparing fractions. For comparing multiple groups, we used

the Kruskal-Wallis test (KW) followed by a posthoc Dunn's comparison test. We used a Two-Way ANOVA followed by a Sidak's multiple comparisons test (Two-Way ANOVA) to compare treatment effects at multiple time points. We have indicated the used tests in the figure legends. Differences between control and treatment were considered significant when $p < 0.05$ (*, $p < 0.05$; **, $p < 0.01$; ***, $p < 0.001$). In all figure legends and text, N indicates the number of independent experiments, and n indicates the number of axons/images analyzed.

ACKNOWLEDGEMENTS

We would like to thank G. Szábo for kindly providing the GAD65-GFP mice, H.Y. Hu and R. van Dorland for technical support, S. Paradis for helpful comments and scientific discussions and A. Akhmanova, G.G. Turrigiano and R.J. Pasterkamp for critically reading the manuscript. This work was supported by the People Programme (Marie Curie Actions) of the European Union's Seventh Framework Programme FP7/2007-2013/ under REA grant agreement 289581 (C.P.F.), a Marie Curie Reintegration Grant 256284 (C.J.W.) and the Netherlands Organization for Scientific Research (NWO-VIDI, C.J.W., NWO-VICI, C.C.H.).

AUTHOR CONTRIBUTIONS

C.P.F. and C.J.W. designed the research. C.P.F. performed the experiments and analyzed the results. T.B. contributed to data in Figure 2H-I and S1F-G. L.S contributed to data in figure 4B,D,F and S2A-E. P.B.H. provided the nanobody. C.P.F., C.C.H. and C.J.W. wrote the manuscript. C.J.W. coordinated and supervised the research.

COMPETING FINANCIAL INTERESTS

The authors declare no competing financial interests.

REFERENCES

BLECKERT, A., PHOTOWALA, H. & ALFORD, S. 2012. Dual pools of actin at presynaptic terminals. *J Neurophysiol,* 107**,** 3479-92.

CHEN, S. X., KIM, A. N., PETERS, A. J. & KOMIYAMA, T. 2015. Subtype-specific plasticity of inhibitory circuits in motor cortex during motor learning. *Nat Neurosci,* 18**,** 1109-15.

CHIA, P. H., CHEN, B., LI, P., ROSEN, M. K. & SHEN, K. 2014. Local F-actin network links synapse formation and axon branching. *Cell,* 156**,** 208-20.

CINGOLANI, L. A. & GODA, Y. 2008. Actin in action: the interplay between the actin cytoskeleton and synaptic efficacy. *Nat Rev Neurosci,* 9**,** 344-56.

DOBIE, F. A. & CRAIG, A. M. 2011. Inhibitory synapse dynamics: coordinated presynaptic and postsynaptic mobility and the major contribution of recycled vesicles to new synapse formation. *J Neurosci,* 31**,** 10481-93.

EAGLESON, K. L., MILNER, T. A., XIE, Z. & LEVITT, P. 2013. Synaptic and extrasynaptic location of the receptor tyrosine kinase met during postnatal development in the mouse neocortex and hippocampus. *J Comp Neurol,* 521**,** 3241-59.

ESTEVES DA SILVA, M., ADRIAN, M., SCHATZLE, P., LIPKA, J., WATANABE, T., CHO, S., FUTAI, K., WIERENGA, C. J., KAPITEIN, L. C. & HOOGENRAAD, C. C. 2015. Positioning of AMPA Receptor-Containing Endosomes Regulates Synapse Architecture. *Cell Rep,* 13**,** 933-43.

FRIAS, C. P. & WIERENGA, C. J. 2013. Activity-dependent adaptations in inhibitory axons. *Front Cell Neurosci,* 7**,** 219.

FROEMKE, R. C. 2015. Plasticity of cortical excitatory-inhibitory balance. *Annu Rev Neurosci,* 38**,** 195-219.

FROEMKE, R. C., MERZENICH, M. M. & SCHREINER, C. E. 2007. A synaptic memory trace for cortical receptive field plasticity. *Nature,* 450**,** 425-9.

FU, Y., WU, X., LU, J. & HUANG, Z. J. 2012. Presynaptic GABA(B) Receptor Regulates Activity-Dependent Maturation and Patterning of Inhibitory Synapses through Dynamic Allocation of Synaptic Vesicles. *Front Cell Neurosci,* 6**,** 57.

GANGULY, A., TANG, Y., WANG, L., LADT, K., LOI, J., DARGENT, B., LETERRIER, C. & ROY, S. 2015. A dynamic formin-dependent deep F-actin network in axons. *J Cell Biol,* 210**,** 401-17.

HENSCH, T. K. 2005. Critical period plasticity in local cortical circuits. *Nat Rev Neurosci,* 6**,** 877-88.

HEUKERS, R., ALTINTAS, I., RAGHOENATH, S., DE ZAN, E., PEPERMANS, R., ROOVERS, R. C., HASELBERG, R., HENNINK, W. E., SCHIFFELERS, R. M., KOK, R. J. & VAN BERGEN EN HENEGOUWEN, P. M. 2014. Targeting hepatocyte growth factor receptor (Met) positive tumor cells using internalizing nanobody-decorated albumin nanoparticles. *Biomaterials,* 35**,** 601-10.

HONKURA, N., MATSUZAKI, M., NOGUCHI, J., ELLIS-DAVIES, G. C. & KASAI, H. 2008. The subspine organization of actin fibers regulates the structure and plasticity of dendritic spines. *Neuron,* 57**,** 719-29.

JUDSON, M. C., BERGMAN, M. Y., CAMPBELL, D. B., EAGLESON, K. L. & LEVITT, P. 2009. Dynamic gene and protein expression patterns of the autism-associated met receptor tyrosine kinase in the developing mouse forebrain. *J Comp Neurol,* 513**,** 511-31.

KECK, T., SCHEUSS, V., JACOBSEN, R. I., WIERENGA, C. J., EYSEL, U. T., BONHOEFFER, T. & HUBENER, M. 2011. Loss of sensory input causes rapid structural changes of inhibitory neurons in adult mouse visual cortex. *Neuron,* 71**,** 869-82.

KURIU, T., YANAGAWA, Y. & KONISHI, S. 2012. Activity-dependent coordinated mobility of hippocampal inhibitory synapses visualized with presynaptic and postsynaptic tagged-molecular markers. *Mol Cell Neurosci,* 49**,** 184-95.

KUZIRIAN, M. S., MOORE, A. R., STAUDENMAIER, E. K., FRIEDEL, R. H. & PARADIS, S. 2013. The class 4 semaphorin Sema4D promotes the rapid assembly of GABAergic synapses in rodent hippocampus. *J Neurosci,* 33**,** 8961-73.

LIM, C. S. & WALIKONIS, R. S. 2008. Hepatocyte growth factor and c-Met promote dendritic maturation during hippocampal neuron differentiation via the Akt pathway. *Cell Signal,* 20**,** 825-35.

LO, F. S., ERZURUMLU, R. S. & POWELL, E. M. 2016. Insulin-Independent GABAA Receptor-Mediated Response in the Barrel Cortex of Mice with Impaired Met Activity. *J Neurosci,* 36**,** 3691-7.

LOPEZ-BENDITO, G., STURGESS, K., ERDELYI, F., SZABO, G., MOLNAR, Z. & PAULSEN, O. 2004. Preferential origin and layer destination of GAD65-GFP cortical interneurons. *Cereb Cortex,* 14**,** 1122-33.

MARTINS, G. J., SHAHROKH, M. & POWELL, E. M. 2011. Genetic disruption of Met signaling impairs GABAergic striatal development and cognition. *Neuroscience,* 176**,** 199-209.

MÜLLNER, F. E., WIERENGA, C. J. & BONHOEFFER, T. 2015. Precision of Inhibition: Dendritic Inhibition by Individual GABAergic Synapses on Hippocampal Pyramidal Cells Is Confined in Space and Time. *Neuron,* 87**,** 576-89.

NELSON, J. C., STAVOE, A. K. & COLON-RAMOS, D. A. 2013. The actin cytoskeleton in presynaptic assembly. *Cell Adh Migr,* 7**,** 379-87.

OH, W. C., LUTZU, S., CASTILLO, P. E. & KWON, H. B. 2016. De novo synaptogenesis induced by GABA in the developing mouse cortex. *Science,* 353**,** 1037-1040.

OINUMA, I., ISHIKAWA, Y., KATOH, H. & NEGISHI, M. 2004. The Semaphorin 4D receptor Plexin-B1 is a GTPase activating protein for R-Ras. *Science,* 305**,** 862-5.

PARADIS, S., HARRAR, D. B., LIN, Y., KOON, A. C., HAUSER, J. L., GRIFFITH, E. C., ZHU, L., BRASS, L. F., CHEN, C. & GREENBERG, M. E. 2007. An RNAi-based approach identifies molecules required for glutamatergic and GABAergic synapse development. *Neuron,* 53**,** 217-32.

PENG, Y., HUENTELMAN, M., SMITH, C. & QIU, S. 2013. MET receptor tyrosine kinase as an autism genetic risk factor. *Int Rev Neurobiol,* 113**,** 135-65.

PICCIOLI, Z. D. & LITTLETON, J. T. 2014. Retrograde BMP signaling modulates rapid activity-dependent synaptic growth via presynaptic LIM kinase regulation of cofilin. *J Neurosci,* 34**,** 4371-81.

QIU, S., LU, Z. & LEVITT, P. 2014. MET receptor tyrosine kinase controls dendritic complexity, spine morphogenesis, and glutamatergic synapse maturation in the hippocampus. *J Neurosci,* 34**,** 16166-79.

RAISSI, A. J., STAUDENMAIER, E. K., DAVID, S., HU, L. & PARADIS, S. 2013. Sema4D localizes to synapses and regulates GABAergic synapse development as a membrane-bound molecule in the mammalian hippocampus. *Mol Cell Neurosci,* 57**,** 23-32.

REX, C. S., CHEN, L. Y., SHARMA, A., LIU, J., BABAYAN, A. H., GALL, C. M. & LYNCH, G. 2009. Different Rho GTPase-dependent signaling pathways initiate sequential steps in the consolidation of long-term potentiation. *J Cell Biol,* 186**,** 85-97.

SABO, S. L., GOMES, R. A. & MCALLISTER, A. K. 2006. Formation of presynaptic terminals at predefined sites along axons. *J Neurosci,* 26**,** 10813-25.

SCHUEMANN, A., KLAWITER, A., BONHOEFFER, T. & WIERENGA, C. J. 2013. Structural plasticity of GABAergic axons is regulated by network activity and GABAA receptor activation. *Front Neural Circuits,* 7**,** 113.

SHI, W., KUMANOGOH, A., WATANABE, C., UCHIDA, J., WANG, X., YASUI, T., YUKAWA, K., IKAWA, M., OKABE, M., PARNES, J. R., YOSHIDA, K. & KIKUTANI, H. 2000. The class IV semaphorin CD100 plays nonredundant roles in the immune system: defective B and T cell activation in CD100-deficient mice. *Immunity,* 13**,** 633-42.

SIDDIQUI, T. J. & CRAIG, A. M. 2011. Synaptic organizing complexes. *Curr Opin Neurobiol,* 21**,** 132-43.

STARAS, K. 2007. Share and share alike: trading of presynaptic elements between central synapses. *Trends Neurosci,* 30**,** 292-8.

SUAREZ, C., CARROLL, R. T., BURKE, T. A., CHRISTENSEN, J. R., BESTUL, A. J., SEES, J. A., JAMES, M. L., SIROTKIN, V. & KOVAR, D. R. 2015. Profilin regulates F-actin network homeostasis by favoring formin over Arp2/3 complex. *Dev Cell,* 32**,** 43-53.

SUN, T., KRISHNAN, R. & SWIERCZ, J. M. 2012. Grb2 mediates semaphorin-4D-dependent RhoA inactivation. *J Cell Sci,* 125**,** 3557-67.

592 SWIERCZ, J. M., KUNER, R., BEHRENS, J. & OFFERMANNS, S. 2002. Plexin-B1 directly interacts with
593 PDZ-RhoGEF/LARG to regulate RhoA and growth cone morphology. *Neuron,* 35**,** 51-63.
594 SWIERCZ, J. M., WORZFELD, T. & OFFERMANNS, S. 2008. ErbB-2 and met reciprocally regulate cellular
595 signaling via plexin-B1. *J Biol Chem,* 283**,** 1893-901.
596 TASAKA, G., NEGISHI, M. & OINUMA, I. 2012. Semaphorin 4D/Plexin-B1-mediated M-Ras GAP activity
597 regulates actin-based dendrite remodeling through Lamellipodin. *J Neurosci,* 32**,** 8293-305.
598 TYNDALL, S. J. & WALIKONIS, R. S. 2006. The receptor tyrosine kinase Met and its ligand hepatocyte
599 growth factor are clustered at excitatory synapses and can enhance clustering of synaptic
600 proteins. *Cell Cycle,* 5**,** 1560-8.
601 VILLA, K. L., BERRY, K. P., SUBRAMANIAN, J., CHA, J. W., CHAN OH, W., KWON, H. B., KUBOTA, Y., SO,
602 P. T. & NEDIVI, E. 2016. Inhibitory Synapses Are Repeatedly Assembled and Removed at
603 Persistent Sites In Vivo. *Neuron,* 90**,** 662-664.
604 VODRAZKA, P., KOROSTYLEV, A., HIRSCHBERG, A., SWIERCZ, J. M., WORZFELD, T., DENG, S., FAZZARI,
605 P., TAMAGNONE, L., OFFERMANNS, S. & KUNER, R. 2009. The semaphorin 4D-plexin-B
606 signalling complex regulates dendritic and axonal complexity in developing neurons via
607 diverse pathways. *Eur J Neurosci,* 30**,** 1193-208.
608 WIERENGA, C. J. 2016. Live imaging of inhibitory axons: Synapse formation as a dynamic trial-and-
609 error process. *Brain Res Bull*.
610 WIERENGA, C. J., BECKER, N. & BONHOEFFER, T. 2008. GABAergic synapses are formed without the
611 involvement of dendritic protrusions. *Nat Neurosci,* 11**,** 1044-52.
612 WIERENGA, C. J., MÜLLNER, F. E., RINKE, I., KECK, T., STEIN, V. & BONHOEFFER, T. 2010. Molecular
613 and electrophysiological characterization of GFP-expressing CA1 interneurons in GAD65-GFP
614 mice. *PLoS One,* 5**,** e15915.

FIGURES

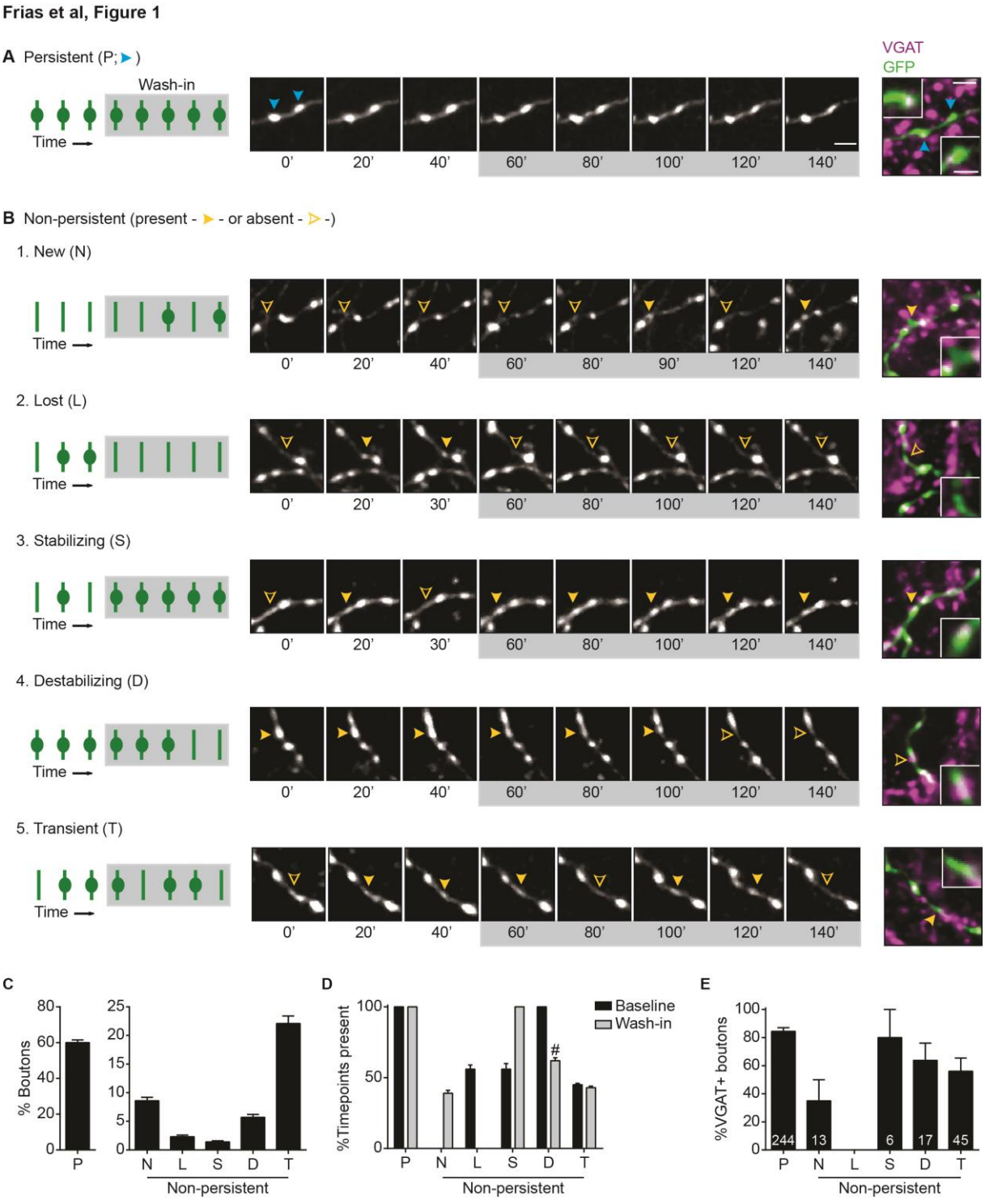

Figure 1. Classification of presynaptic inhibitory boutons by their dynamics.

(A) Time-lapse two-photon images of two inhibitory boutons (blue arrowheads) along a GAD65-GFP-labeled axon in the CA1 region of the hippocampus. These boutons were present at all time points, and therefore categorized as persistent boutons. Only every second image is shown for clarity. On the right, the same region is shown after fixation and

staining against vesicular GABA transporter (VGAT, magenta). The zoom shows a single optical plane through the bouton to demonstrate overlap (white) of VGAT and GFP boutons. Time in minutes. Scale bars 2 µm and 1 µm (zoom).

(B1-5) Same as in A, showing examples of new (B1; absent during baseline), lost (B2; absent during wash-in), stabilizing (B3; non-persistent during baseline, and persistent during wash-in), destabilizing (B4; persistent during the baseline, and non-persistent during the wash-in) and transient (B5; non-persistent during both baseline and wash-in) boutons. Filled yellow arrowheads indicate that the bouton is present, and empty yellow arrowheads indicate that the bouton is absent at the time point shown.

(C) Number of persistent and non-persistent boutons (N – new; L – lost; S – stabilizing; D – destabilizing; T – transient) as fraction of boutons that appeared during total imaging period.

(D) Percentage of time points in which boutons were present during baseline (black) and wash-in (light green) periods. #: values for D were significantly different from N and T ($p < 0.01$; χ^2).

(E) Fraction of boutons positive for VGAT per axon. Numbers indicate the number of boutons analyzed per group.

Confocal images are maximum intensity projections of 5-8 z stacks, while two-photon images are maximum intensity projections of 13-15 z stacks.

In C and D: data from 92 axons from 24 independent experiments. In E: data from 21 axons from 5 independent experiments.

Frias et al, Figure 2

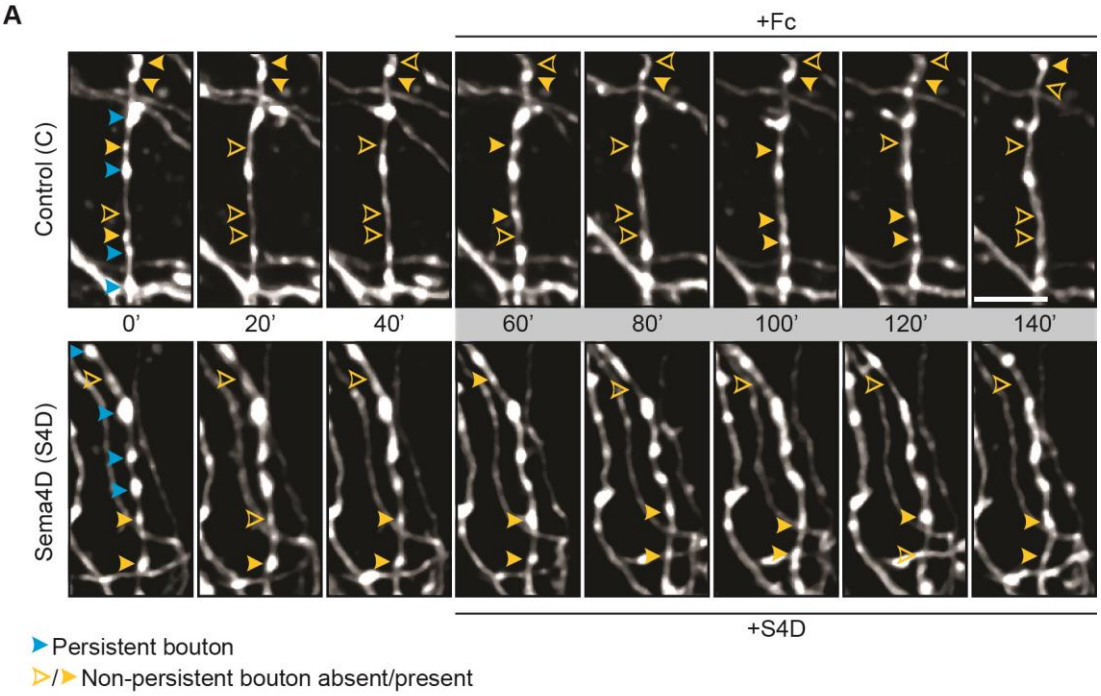

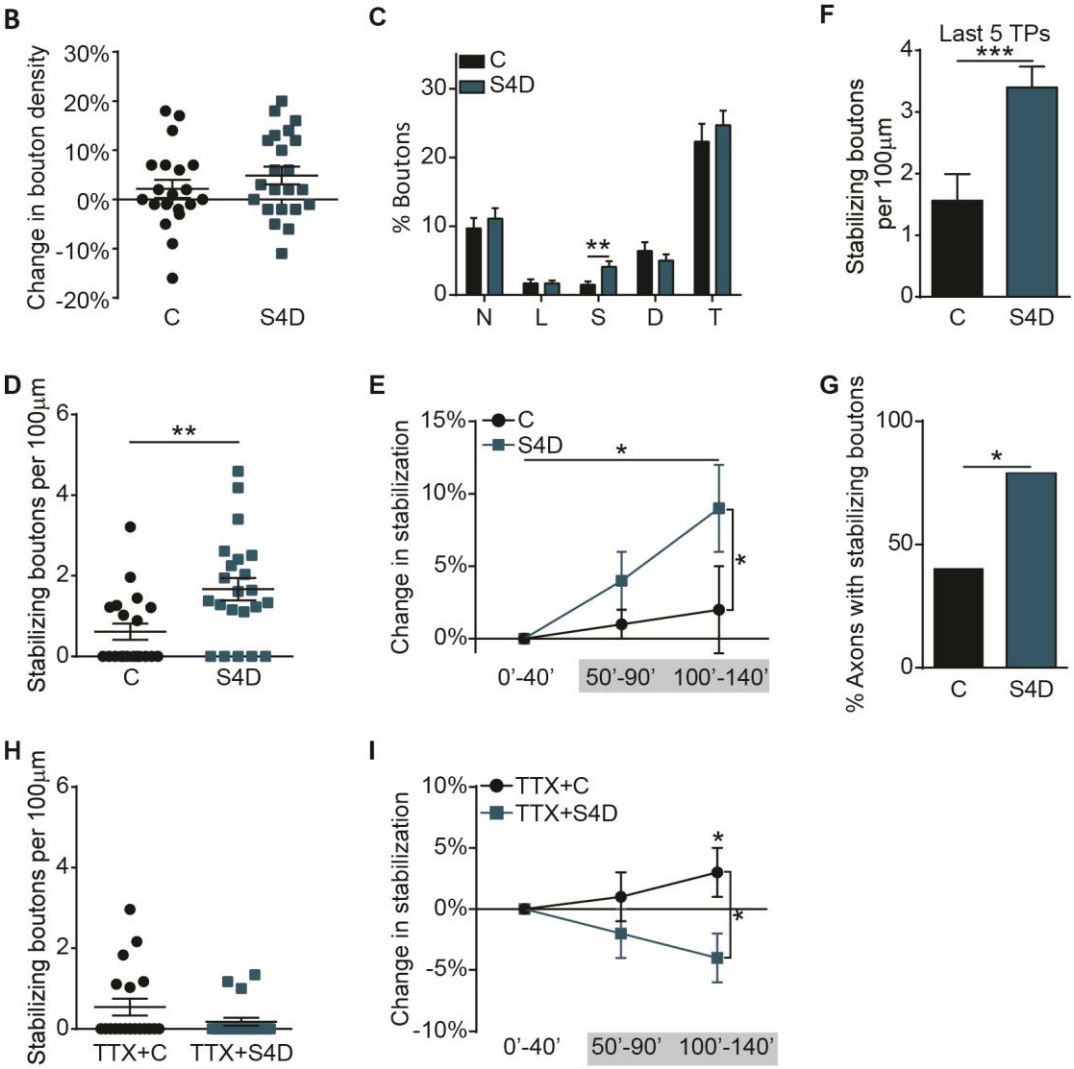

643

Figure 2. Sema4D treatment promotes inhibitory bouton stabilization.

(A) Time-lapse two-photon images of GFP-labeled inhibitory axons in the CA1 region of the hippocampus during baseline (5 time points) and wash-in (10 time points; grey box) of 1 nM Fc - control (C; upper panel) or 1 nM Sema4D-Fc (S4D; bottom panel). Only every second image is shown for clarity. The images show persistent (blue arrowheads), and non-persistent boutons (yellow arrowheads). Filled arrowheads indicate that the bouton is present, and empty arrowheads indicate that the bouton is absent at that time point. Images are maximum intensity projections of 11-18 z stacks. Time in minutes. Scale bar 5 µm.

(B) Change in mean bouton density during the last 5 time points compared to baseline after wash-in of Fc (C) or S4D. Each dot represents an individual axon; $p = 0.41$ (MW).

(C) Fraction of total boutons belonging to the five subgroups of non-persistent boutons in control and Sema4D-treated axons: N – new; L – lost; S – stabilizing; D – destabilizing; T - transient. ** $p < 0.01$ (MW per subgroup).

(D) Density of stabilizing boutons in Fc- and S4D-treated axons. Each dot represents an individual axon. ** $p < 0.01$ (MW).

(E) Stabilization of inhibitory boutons, as determined by the change (compared to baseline) in density of boutons that were present at 5 consecutive time points during the imaging period: 0'-40' (baseline), 50'-90' (wash-in) and 100'-140' (wash-in). Two-way ANOVA analysis showed a significant effect of both treatment and time. * $p < 0.05$ (Two-Way ANOVA).

(F) Density of boutons that stabilized in the last 5 time points (TPs). *** $p < 0.001$ (MW).

(G) Fraction of axons with stabilizing boutons. * $p < 0.05$ (χ^2).

(H,I) Same as in D and E, but in the presence of 0.5 µM TTX. Two-way ANOVA analysis showed a significant effect of treatment. * $p < 0.05$ (Two-Way ANOVA).

Data in B-H from 20 control axons (N=6) and 22 S4D-treated axons (N=5), and in H-I from 19 control axons (N=5) and 20 S4D-treated axons (N=5).

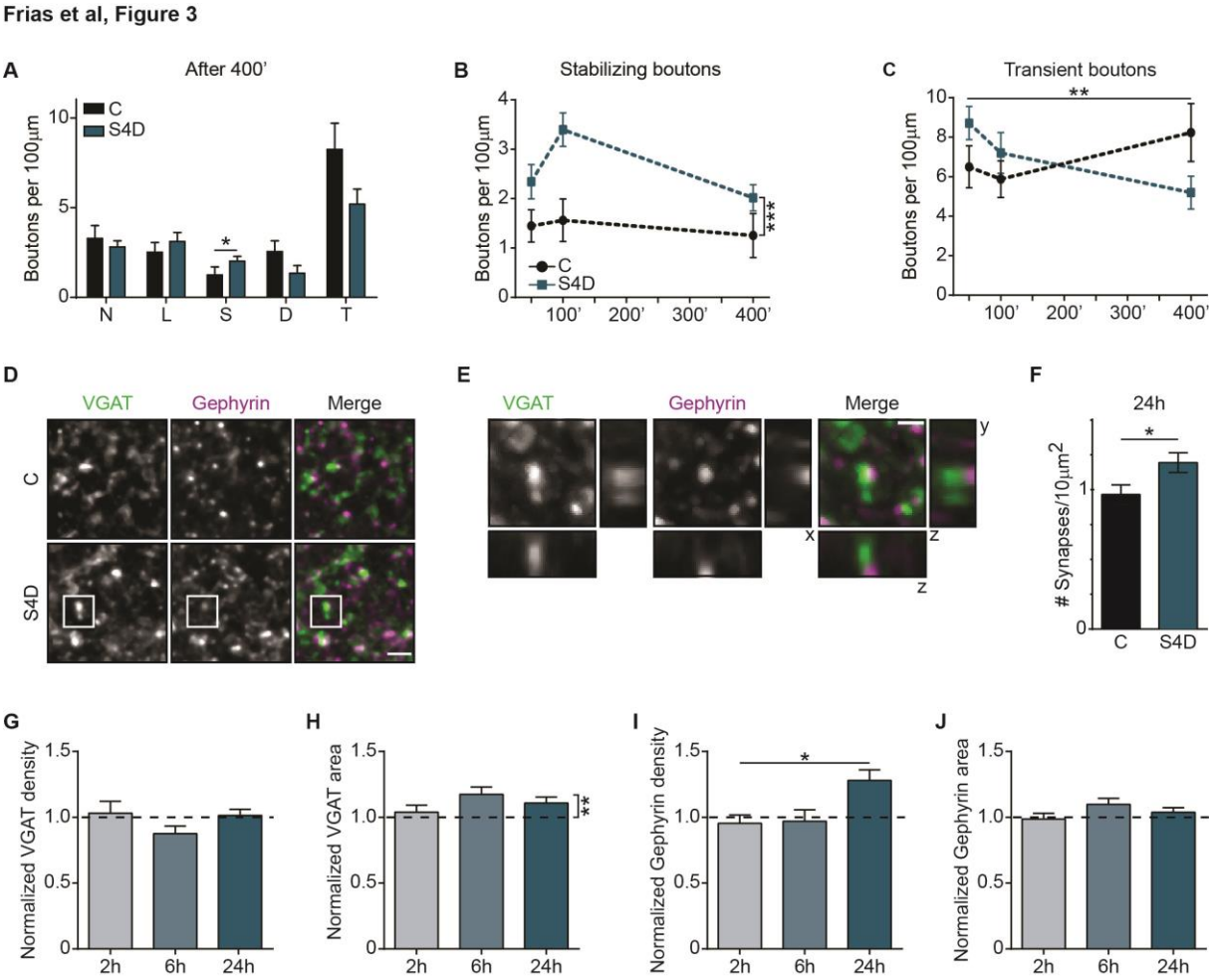

Figure 3. Sema4D increases overall inhibitory synaptic density.

(A) Density of non-persistent boutons (N – new; L – lost; S – stabilizing; D – destabilizing; T – transient) after treatment with 1 nM Fc (control; C) or 1 nM Sema4D-Fc (S4D) for 6 hours (400 minutes of total treatment). * $p < 0.05$ (MW per subgroup).

(B) Density of stabilizing boutons after treatment with Fc or S4D for 50, 100 and 400 minutes. Two-way ANOVA analysis showed that S4D increased density independent of time. *** $p < 0.001$ (Two-Way ANOVA).

(C) Same as B, but for transient boutons. Two-Way ANOVA analysis indicated a significant interaction between treatment and time in D. ** $p < 0.01$ (Two-Way ANOVA).

(D) Representative images of CA1 dendritic area of GAD65-GFP hippocampal slices treated with 1 nM Fc (C) or 1 nM Sema4D-Fc (S4D) for 24 h, and immunostained for VGAT (green) and gephyrin (magenta). Images are average intensity projections of 5 z stacks. Scale bar 2 µm.

(E) Example of an inhibitory synapse (white box in D), identified as the apposition of VGAT (green) and gephyrin (magenta) puncta. The respective xz and yz projections show the

close apposition of the two markers. Images are maximum intensity projections of 6 z stacks. Scale bar 1 µm.

(F) Density of inhibitory synapses in slices treated with Fc or Sema4D for 24 h. * $p < 0.05$ (MW).

(G) Normalized density of presynaptic vesicular GABA transporter (VGAT) puncta (after treatment with 1 nM S4D for 2 h, 6 h and 24 h. Dotted line represents control (treatment with 1nM Fc for 2 h, 6 h and 24 h).

(H) Same as in G, but for VGAT puncta area. Two-way ANOVA analysis showed that S4D treatment increased VGAT area independent of time. ** $p < 0.01$ (Two-Way ANOVA).

(I-J) Same as in G-H, but for density (I) and area (J) of postsynaptic gephyrin puncta. Two-way ANOVA analysis showed an interaction between treatment and time. * $p < 0.05$ (Two-Way ANOVA).

In A, data from 15 control axons (N=4) and 17 S4D-treated axons (N=4), and in D-J from 15-20 control images (N=3-4) and 15-20 S4D images (N=3-4).

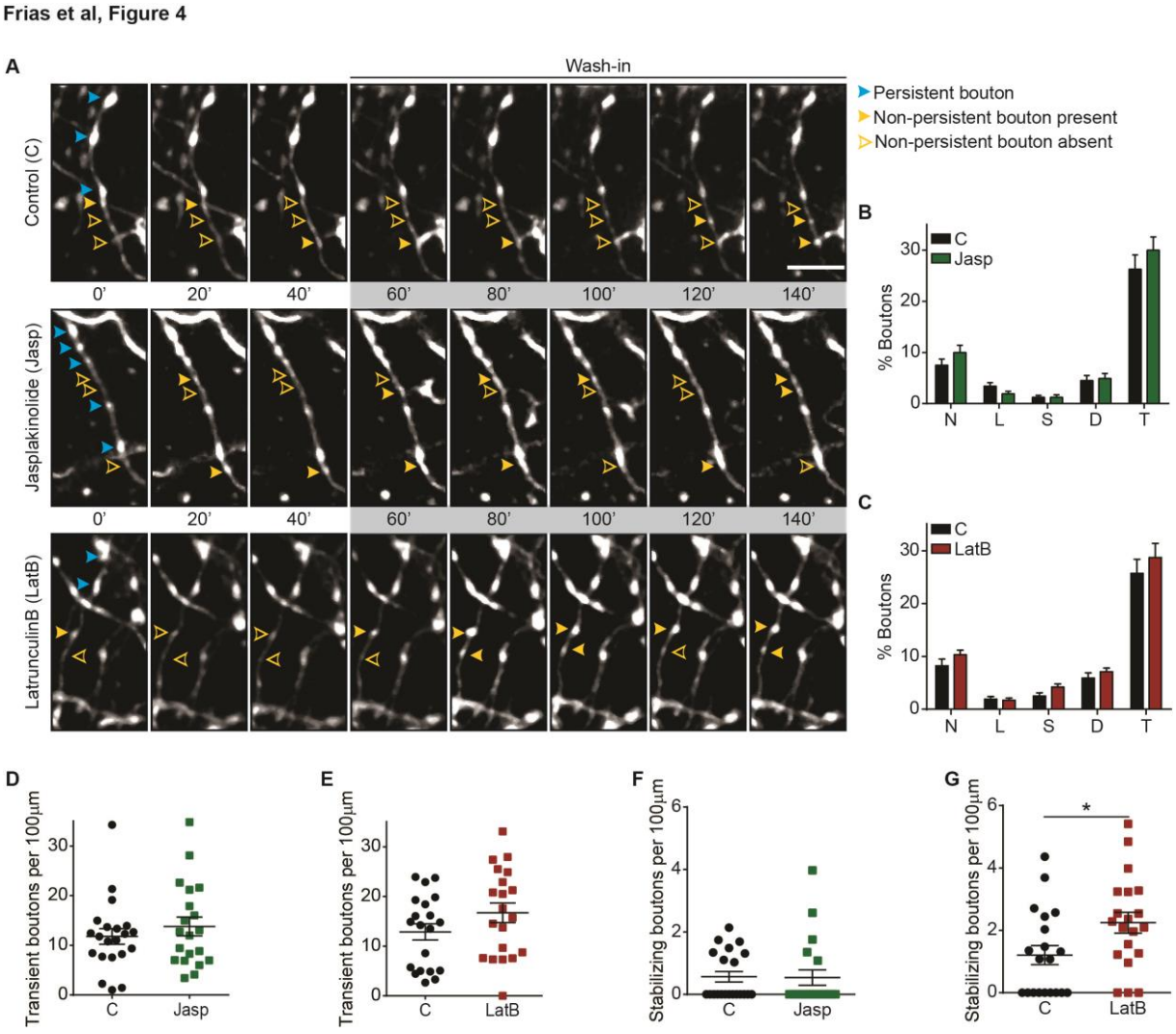

Figure 4. Inhibitory bouton dynamics are regulated by actin.

(A) Time-lapse two-photon images of GAD65-GFP-labeled axons in the CA1 region of the hippocampus during baseline (5 time points) and wash-in (10 time points; grey box) of DMSO - control (C; upper panel), 200 nM Jasplakinolide (Jasp; middle panel) or 100 nM LatrunculinB (LatB; bottom panel). Only every second image is shown for clarity. Persistent and non-persistent boutons are indicated as in Figure 2. Images are maximum intensity projections of 12-14 z stacks. Time in minutes. Scale bar 5 µm.

(B) Fraction of total number of boutons comprised by the five subgroups of non-persistent boutons (N – new; L – lost; S – stabilizing; D – destabilizing; T – transient) control and Jasp-treated axons.

(C) Same as in B, but for control and LatB-treated axons.

(D) Density of transient boutons in slices treated with DMSO and Jasp. Each dot represents an individual axon. $p = 0.57$ (MW).

(E) Same as D, but for control and LatB-treated axons. $p = 0.13$ (MW).

(F) Density of stabilizing boutons in control and Jasp-treated axons. $p = 0.55$ (MW).

(G) Same as F, but for control and LatB-treated axons. * $p < 0.05$ (MW).

Data from 21 control axons (N=5) and 20 Jasp-treated axons (N=5) in B, D and F, and from 20 control axons (N=5) and 20 LatB-treated axons (N=5) in C, E and G.

Frias et al, Figure 5

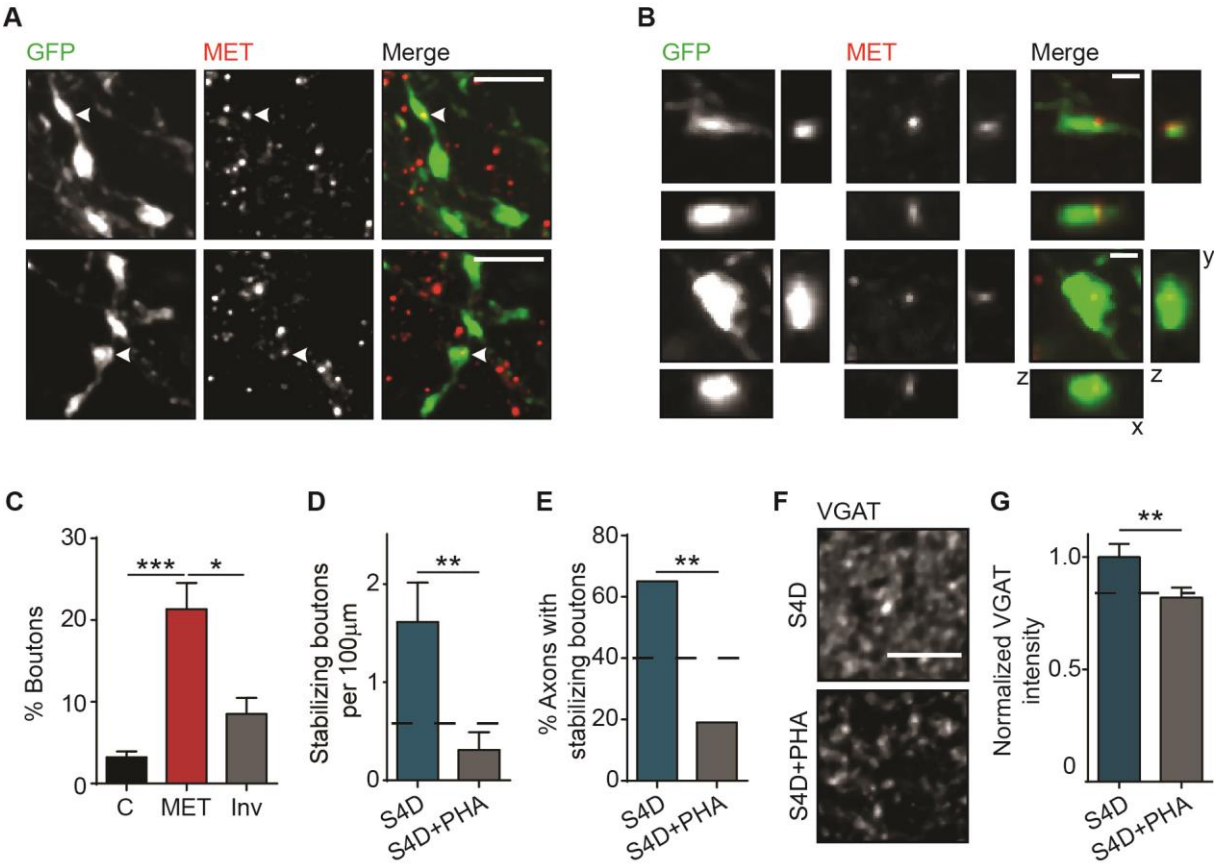

Figure 5. Inhibitory bouton stabilization by Sema4D requires MET.

(A) Representative images of GFP-labeled inhibitory boutons (green) in hippocampal slices, stained for MET (red). Images are maximum intensity projections of 6 z stacks. White arrows indicate boutons MET enrichments in GFP-labeled boutons. Scale bar 5 µm.

(B) Example of two inhibitory boutons (green) in hippocampal slices showing enrichment in MET (red), and the respective xz and yz projections. Images are maximum intensity projections of 6 z stacks. Scale bar 1 µm.

(C) Fraction of GFP boutons positive for MET. Aspecific staining was determined by anti-myc staining without nanobody ('C') and random co-localization was determined by inverting the MET channel ('Inv'). * $p < 0.05$, *** $p < 0.001$ (KW).

(D) Density of stabilizing boutons in slices treated with a combination of 1 nM Sema4D/DMSO (S4D) or 1 nM Sema4D/1 µM PHA-665752 (S4D+PHA). Dotted line represents control values. ** $p < 0.01$ (MW).

(E) Fraction of axons with stabilizing boutons. Dotted line represents control values. ** $p < 0.01$ (χ^2).

735 **(F)** Representative images of hippocampal slices treated with S4D (upper panel) or
736 S4D+PHA (bottom panel) for 100', and stained for presynaptic VGAT. Images are average
737 intensity projections of 5 z stacks. Scale bar 5 µm.
738 **(G)** Normalized mean area staining intensity for VGAT. Control value is indicated with
739 dotted line. ** $p < 0.01$ (MW).
740 In C, data from 10 control images (N=2), and 12 images in Met and inverted group (N=3), in
741 D-E from 17 S4D-treated axons (N=4) and 16 S4D+PHA-treated axons (N=4), and in G from 16
742 images of S4D-treated slices (N=3) and 23 images of S4D+PHA-treated slices (N=4).

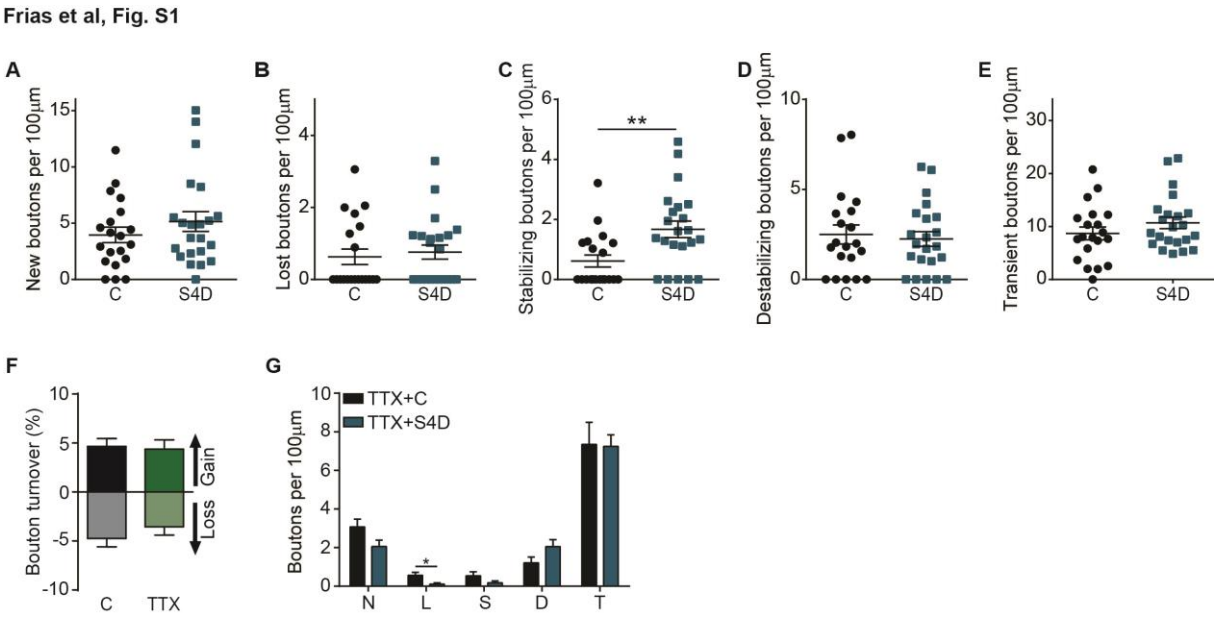

Figure S1. Effect of Sema4D treatment on inhibitory bouton dynamics

(A) Density of new boutons in axons treated with 1 nM Fc (C) and 1 nM Sema4D-Fc (S4D). $p = 0.41$ (MW).

(B-E) Same as in A, but for lost (B; $p = 0.61$ (MW)), stabilizing (C), destabilizing (D; $p = 0.84$ (MW)) and transient (E; $p = 0.33$ (MW)). ** $p < 0.01$ (MW).

(F) Mean instantaneous bouton turnover (average of last 5 time points) in control and TTX-treated slices.

(G) Density of boutons belonging to the five subgroups of non-persistent boutons in control (Fc) and Sema4D (S4D)-treated axons in the presence of 0.5 µM TTX: N – new; L – lost; S – stabilizing; D – destabilizing; T - transient. * $p < 0.05$ (MW per subgroup).

In A-E, data from 20 control axons (N=6) and 22 S4D-treated axons (N=5), in F from 17 control axons (N=5) and 17 TTX-treated axons (N=5), and in G from 19 control axons (N=5) and 20 S4D-treated axons (N=5).

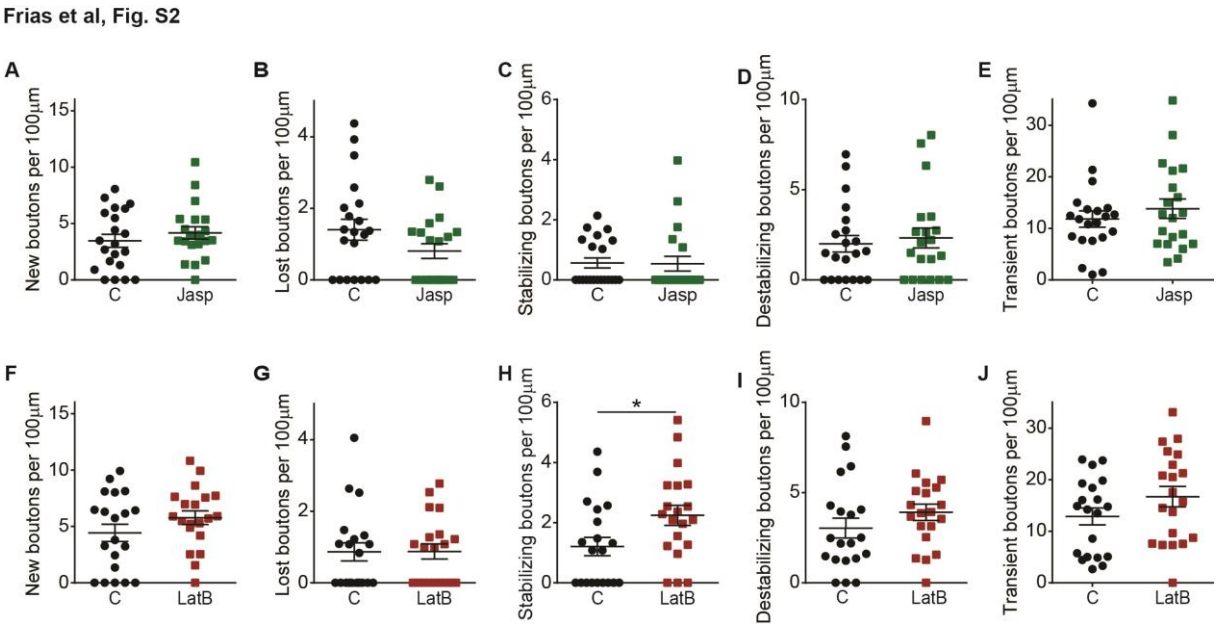

Figure S2. Effect of actin regulating drugs on inhibitory bouton dynamics.

(A) Density of new boutons in control (C) and Jasplakinolide (Jasp; 200 nM)-treated slices. $p = 0.45$ (MW).

(B-E) Same as in A, but for lost (B; $p = 0.14$ (MW)), stabilizing (C; $p = 0.55$ (MW)), destabilizing (D; $p = 0.68$ (MW)) and transient (E; $p = 0.57$ (MW)).

(F-J) Same as in A-E, but for control (C) and LatrunculinB (LatB; 100 nM)-treated slices. * $p < 0.05$ (MW).

Data from 21 control axons (N=5) and 20 Jasp-treated axons (N=5) in A-E, from 20 control axons (N=5) and 20 LatB-treated axons (N=5) in F-J.

Frias et al, Fig. S3

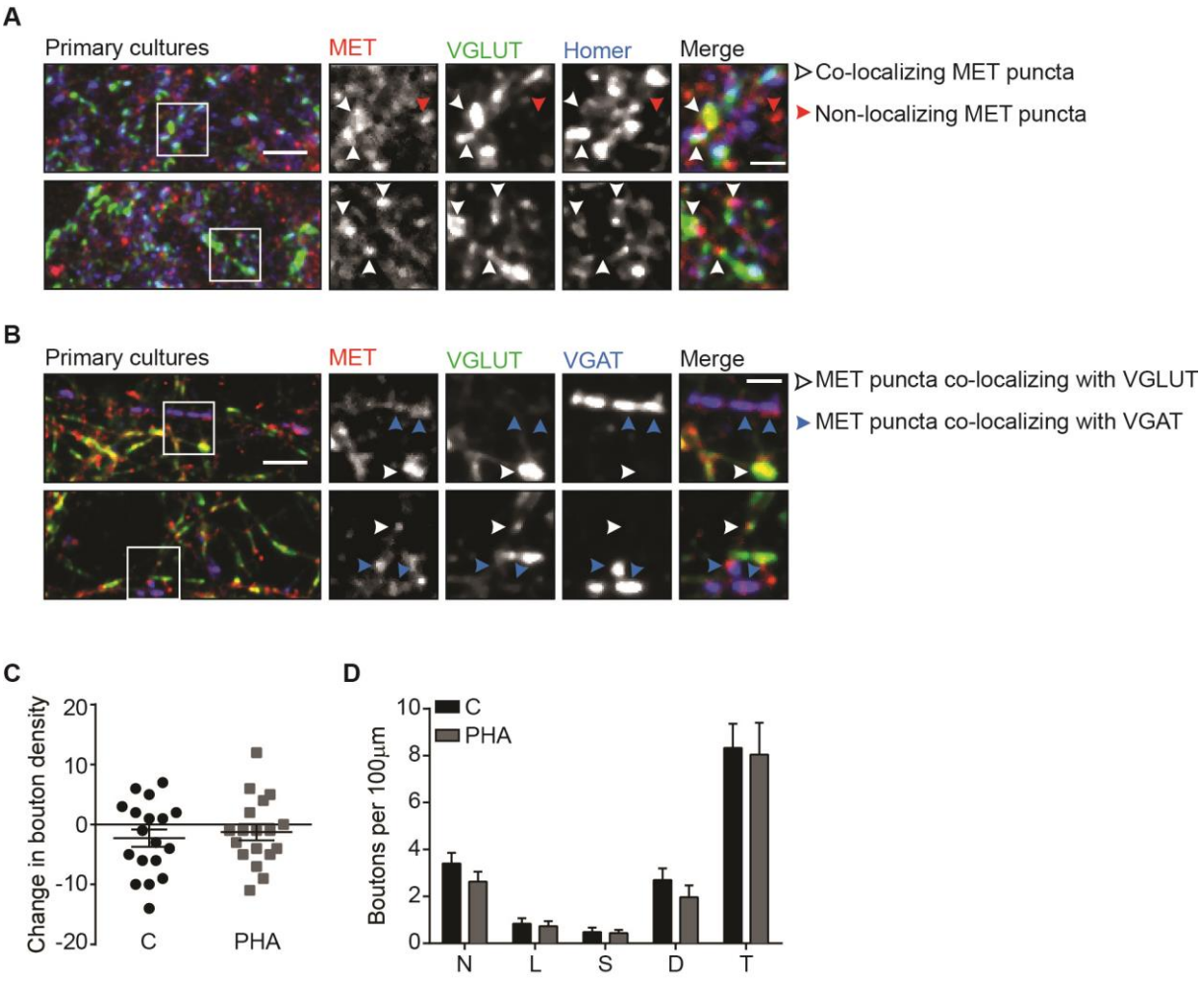

Figure S3. Enrichment of MET at synapses, and effects of MET inhibition on inhibitory bouton dynamics.

(A) Images of primary cultures of hippocampal neurons immunostained for MET (red) and markers for excitatory synapses: presynaptic vesicular glutamate transporter (VGLUT; green) and postsynaptic Homer (blue). White arrows highlight MET puncta co-localizing with one or both markers. Red arrows indicate MET puncta that do not localize. Images are maximum intensity projections of 13 stacks. Scale bar 5 µm (overview) and 2 µm (zoom).

(B) Same as A, but neurons were stained with MET nanobody (red) and markers for excitatory presynapses (presynaptic VGLUT; green) and inhibitory presynapses (presynaptic vesicular GABA transporter VGAT; blue). White arrows indicate MET co-localizing with VGLUT and blue arrows indicate MET co-localizing with VGAT. Images are maximum intensity projections of 12 stacks. Scale bar 5 µm (overview) and 2 µm (zoom).

780 **(C)** Change in mean bouton density compared to baseline after wash-in of control (DMSO)
781 or 1 µM of PHA-665752 (PHA). Each dot represents an individual axon; $p = 0.78$ (MW).
782 **(D)** Density of boutons belonging to the five subgroups of non-persistent boutons in
783 control and PHA-treated axons: N – new; L – lost; S – stabilizing; D – destabilizing; T -
784 transient.
785 In C-D, data from 18 control axons (N=4) and 18 PHA-treated axons (N=4).

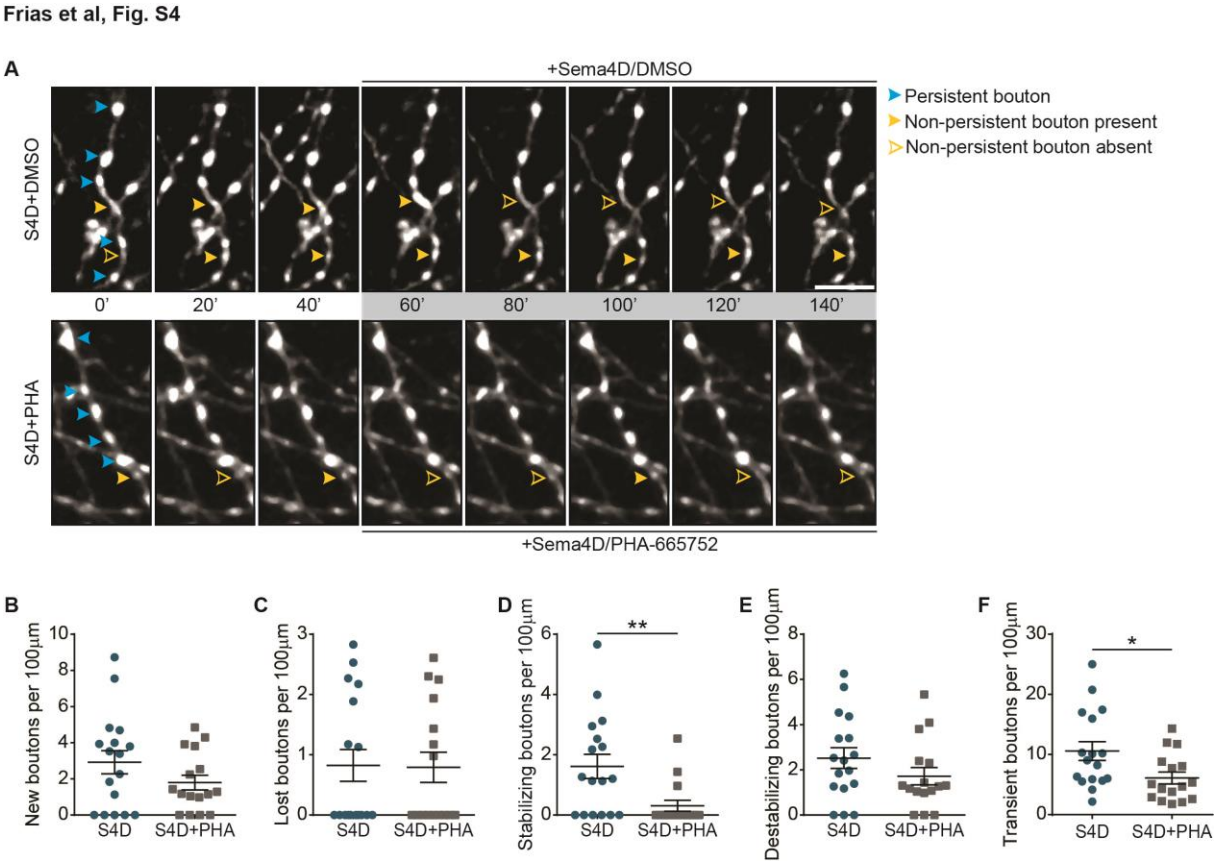

Figure S4. MET inhibition on Sema4D effect on inhibitory bouton dynamics.

(A) Time-lapse two-photon images of GAD65-GFP-labeled axons in organotypic hippocampal slices during wash-in (grey box) of combination of 1 nM Sema4D and DMSO (S4D; upper panel) or combination of 1 nM Sema4D with 1 µM PHA-665752 (S4D+PHA; bottom panel). Images are maximum intensity projections of 15-16 z stacks. The images show persistent (blue arrowheads), and non-persistent boutons (yellow arrowheads). Filled arrowheads indicate that the bouton is present, and empty arrowheads indicate that the bouton is absent at that time point. Scale bar 5 µm.

(B) Density of new boutons in S4D and S4D+PHA-treated axons. $p = 0.34$ (MW).

(C-F) Same as B, but for lost (C; $p = 1$ (MW)), stabilizing (D) destabilizing (E; $p = 0.14$ (MW)) and transient (F) boutons. * $p < 0.05$, ** $p < 0.01$ (MW).

Data from 17 S4D-treated axons (N=4) and 16 S4D+PHA-treated axons (N=4) in D-G.